analytical chemistry

pubs.acs.org/ac Article

Highly Efficient Electrochemiluminescence of MnS:CdS@ZnS Core–Shell Quantum Dots for Ultrasensitive Detection of MicroRNA

Yu-Ting Yang, Jia-Li Liu, Man-Fei Sun, Ruo Yuan,* and Ya-Qin Chai*

Cite This: *Anal. Chem.* 2022, 94, 6874–6881 Read Online

ACCESS | Metrics & More | Article Recommendations | Supporting Information

ABSTRACT: In this work, a novel electrochemiluminescence (ECL) biosensor was developed for ultrasensitive detection of microRNA let-7a (miRNA let-7a) based on MnS:CdS@ZnS core–shell quantum dots (QDs) as ECL luminophores with high ECL efficiency. Impressively, compared to the CdS:Mn@ZnS QDs prepared by ionic doping with ECL efficiency of 0.87%, MnS:CdS@ZnS QDs synthesized by bimetallic clusters ($Cd_2Mn_2O_4$) doping exhibited high ECL efficiency of up to 15.84% with $S_2O_8^{2-}$ as cathodic coreactant due to the elimination of the dopants size mismatch and "self-purification" effect, which could achieve the surface defect passivation of MnS:CdS@ZnS QDs for effectively improving the ECL emission. Furthermore, with the help of strand displacement amplification (SDA), the trace target miRNA let-7a was able to be converted to a number of output DNA labeled with ferrocene (Fc) to construct an ultrasensitive ECL biosensor. The well-designed ECL biosensor for miRNA let-7a exhibited high stability and excellent sensitivity of a concentration variation from 10 aM to 1 nM and a low detection limit of 4.1 aM, which was further applied to the analysis of miRNA let-7a from cancer cell (MCF-7) lysate. Thus, this strategy provides a novel method to prepare high-efficient ECL emitters for the construction of ECL biosensing platforms in biological fields and clinical diagnosis.

Downloaded via TSINGHUA UNIV on November 10, 2022 at 06:54:02 (UTC).
See https://pubs.acs.org/sharingguidelines for options on how to legitimately share published articles.

MicroRNAs (miRNAs) with approximately 18–25 ribonucleotides, whose abnormal expression are associated with abundant types of cancers, meaning that miRNAs could be employed as biomarkers for clinical diagnosis and disease treatment.[1] Therefore, it is urgent to achieve the accurate and ultrasensitive detection of miRNA in clear diagnosis. Electrochemiluminescence (ECL) technology has played a key role in biological applications owing to the merits of high sensitivity, low background signal, and preferable controllability.[2] Currently, doped quantum dots (QDs) on account of reducing band gap[3] and improving electrical conductivity[4] has been widely used as ECL emitters for sensitive determination of biomolecules (microRNA,[5] proteins,[6] and exosomes[7]). However, compared with the formation energy of the host materials, that of dopants is higher, so that the dopants might not replace the host lattice, called "self-purification" effect,[8,9] resulting in the low concentration of dopants ions in QDs to affect the ECL efficiency of QDs. Herein, as displayed in Scheme 1A, MnS:CdS@ZnS core–shell QDs were synthesized at the expense of bimetallic clusters ($Cd_2Mn_2O_4$) precursor to avoid the problem of dopants size mismatch and attenuate the effect of "self-purification", which exhibited the higher ECL efficiency of up to 15.84% as compared to CdS:Mn@ZnS QDs through ionic doping (0.87%).

Hence, we combined the MnS:CdS@ZnS core/shell structure QDs as ECL emitters and mRNA-powered strand displacement amplification as a signal amplification strategy to construct an ECL "signal-off" biosensor for ultrasensitive detection of target microRNA let-7a (miRNA let-7a) from cancer cells. In Scheme 1B, the magnetic beads were assembled with two types of DNA duplexes, R/S and F*/R*. Impressively, S was labeled with ferrocene (Fc-S), and R* included a loop in the middle that could hybridize with R. With the aid of target miRNA let-7a (T), Fc-S in R/S duplex were gradually displaced to form R/T and release Fc-S simultaneously. Fortunately, in the presence of mRNA as fuel strands (F), amounts of strand displacement events continuously occurred. After F being hybridized with F*, R* was liberated to subsequently hybridize with R for releasing T, which participated in next cycle amplification. Interestingly, above displacement was repeated to release abundant Fc-S (output DNA) for further biosensor construction to effectively improve the conversion efficiency of miRNA let-7a for achieving signal amplification. For the electrode modification in Scheme 1C, first, the luminescent nanocomposite, MnS:CdS@ZnS QDs, provided the strong ECL response ("signal-on" mode). Then, with the help of Probe DNA1 and Probe DNA2, the "Y" structure was built by capturing output DNA on the electrode surface to reduce ECL intensity due to

Received: March 1, 2022
Accepted: April 20, 2022
Published: April 28, 2022

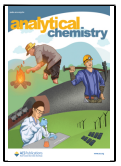

© 2022 American Chemical Society

https://doi.org/10.1021/acs.analchem.2c00970
Anal. Chem. 2022, 94, 6874–6881

Scheme 1. (A) The Preparation of MnS:CdS@ZnS QDs, (B) mRNA-Powered Strand Displacement Amplification, and (C) the Detection Process for MicroRNA let-7a

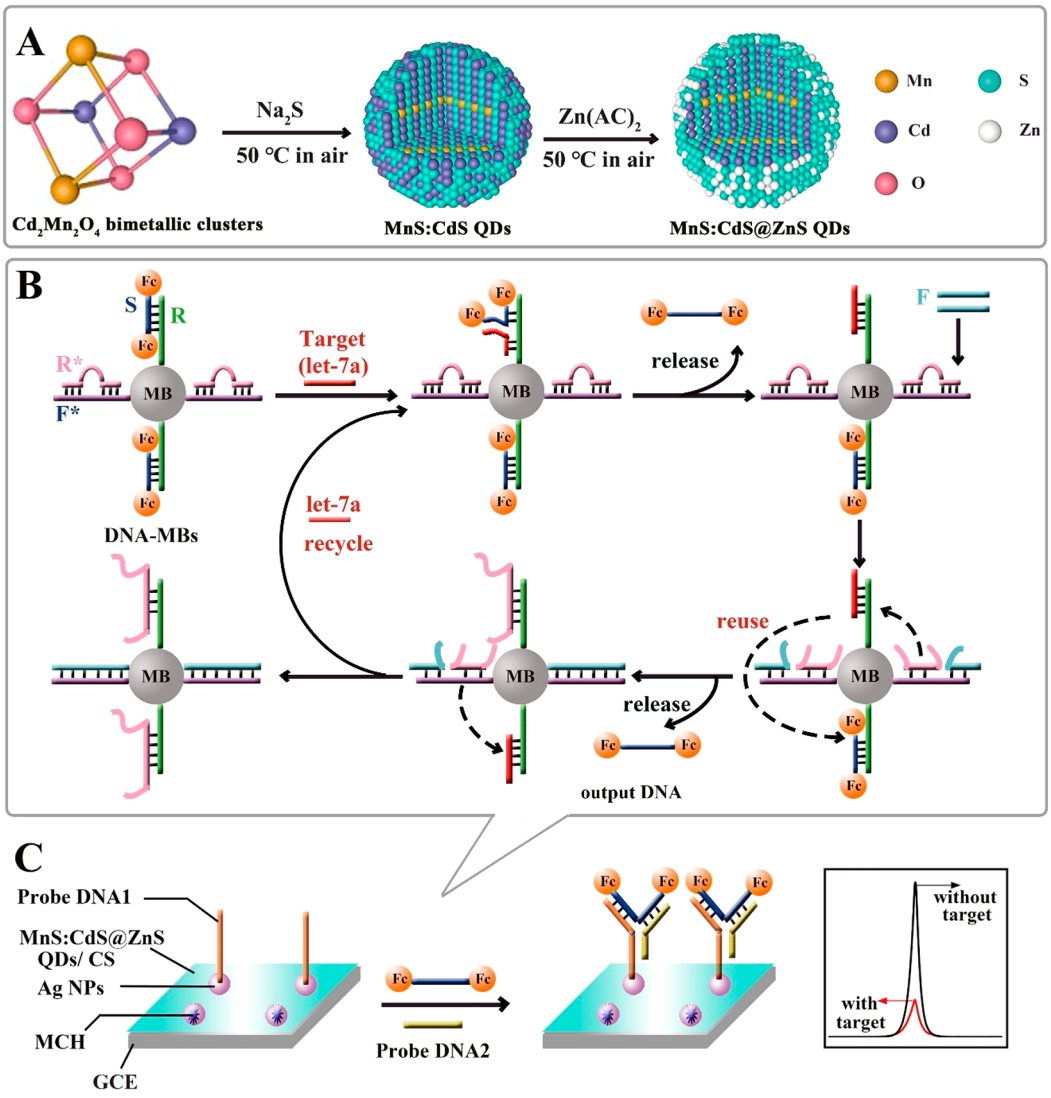

the quenching labels of ferrocene ("signal-off" mode). Thus, the designed ECL biosensor provided a prominent prospect for quantifying miRNA let-7a with a low detection limit of 4.1 aM. Significantly, this biosensor exhibits novel ideas in designing biosensing platforms for ultrasensitive analysis of biomolecules and early cancer diagnosis.

EXPERIMENTAL SECTION

Prepartion of MnS:CdS@ZnS QDs/Chitosan. MnS:CdS@ZnS QDs were successfully obtained via the previous report with minor modification.[10] First, 0.7353 g (6 mmol) of $Mn(Ac)_2{\cdot}2H_2O$ was added to 10.5 mL of distilled water at 50 °C. Then, 5.25 mL of acetonitrile solution containing 0.2763 g (3 mmol) of dipyridyl ketone and 1.5 mL of $NaClO_4$ solution (4.0 M) were added dropwise to the above solution. After 48 h of reflux condensation, white polyhedral crystals were obtained, which were washed and centrifuged with deionized water (12 000 rpm and 5 min) and dried in vacuum freezing to obtain the white powder (Mn_4O_4). The same method was used to synthesize bimetallic clusters $Mn_2Cd_2O_4$ cubane-like cluster building blocks, by replacing 0.7353 g of $Mn(Ac)_2{\cdot}2H_2O$ (6 mmol) to 0.7996 g of $Cd(Ac)_2{\cdot}2H_2O$ (3 mmol) and 0.3676 g of $Mn(Ac)_2{\cdot}2H_2O$ (3 mmol). Subsequently, 0.0614 g of L-glutathione was dissolved in 10 mL of distilled water and the pH of solution was probably adjusted to 8 with NaOH (1 mM) with stirring under 50 °C. Then, 2 mg of Mn_4O_4 and $Na_2S{\cdot}9H_2O$ (0.1 M) were added to above solution. Ten min later, 18 mg of $Mn_2Cd_2O_4$ dissolved in 4 mL of deionized water was quickly added into above solution and reacted for 10 min. Afterward, 0.036 g of $Zn(Ac)_2{\cdot}2H_2O$ dissolved in 6 mL of aqueous water was added into mixture solution at the rate of 0.1 mL per minute. Later, after centrifuging and washing with ethanol three times, MnS:CdS@ZnS QDs were obtained by vacuum drying overnight. Finally, the previously prepared MnS:CdS@ZnS QDs and 0.25% chitosan solution were continuously stirred to obtain MnS:CdS@ZnS QDs/CS solution.

mRNA-Powered Strand Displacement Amplification. For the successful preparation of DNA modified magnetic beads with two types of duplexs, R/S and F*/R*(DNA-MBs), 10 μL of carboxyl modified magnetic beads (MBs) was mixed into 35 μL of EDC solution (80 mM) and reacted for 15 min for activating carboxyl. Then, 35 μL of NHS solution (20 mM), 20 μL of R (10 μL, 10 μM) and F* (10 μL 10 μM),

https://doi.org/10.1021/acs.analchem.2c00970
Anal. Chem. 2022, 94, 6874−6881

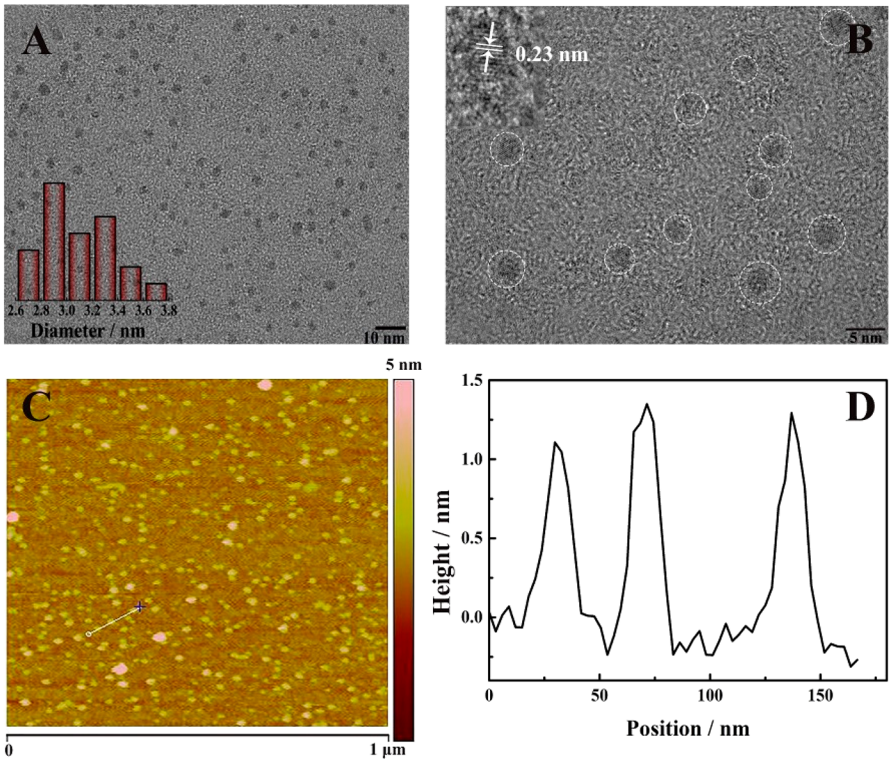

Figure 1. (A) TEM image (inset: particle size distribution image), (B) HRTEM image (inset: the lattice spacing), and (C) AFM graph of MnS:CdS@ZnS QDs. (D) The height profile (AFM) of the line in panel C.

which were both labeled amino group, were added into above solution to stir for 1 h to cross-link through amide bond. After magnetic separation to remove superfluous R and F*, 20 μL solution of S-Fc (10 μM) and R* (10 μM) were simultaneously mixed with above solution. Subsequently, the mixture solution was hybridized at 95 °C for 5 min and then gradually cooled to 37 °C in 2 min per degree and kept for 2 h at 37 °C. After the mixtures were magnetically separated, DNA-MBs were obtained and dispersed in 80 μL of TAE-Mg^{2+} buffer and stored at 4 °C until using. Thereafter, 10 μL of F (50 nM) and 10 μL of target miRNA let-7a (T) with different concentrations (10 nM to 100 aM) were mixed into DNA-MBs solution and reacted for 3 h at 37 °C to carry out the strand displacement amplification. Ultimately, magnetic separation was used to collect the supernatant, which was necessary for output DNA.

Construction of ECL Biosensor. The polished glassy carbon electrode (GCE) was obtained referring to the reported method.[11] Then, in order to modify the electrode, 10 μL of MnS:CdS@ZnS QDs/CS solution and 10 μL of Ag NPs were dropped on the pretreatment GCE to dry at 37 °C for 3 h. In sequence, with the help of Ag−S bond, probe DNA1 (10 μL, 1 μM) was successfully incubated on the dried electrode overnight at 4 °C. Separating excess substances with distilled water, then the resultant electrode was incubated with MCH (10 μL, 5 mM) for 10 min for blocking the nonspecific sites. At last, the assembled electrode was washed with distilled water to remove unbound substances for further use.

Measurement Procedure. Overall, probe DNA2 (5 μL, 1 μM) and output DNA (5 μL) were simultaneously introduced to the prepared electrode and subsequently reacted at 37 °C for 2 h to construct Y structure. The incubated electrode was rinsed with distilled water for discarding extra reagents. Finally, in 30 mM $S_2O_8^{2-}$ solution, the ECL response was obtained by the MPI-E analyzer through the cyclic voltammetry (CV) scaning range of 0 to −2.0 V at the rate of 0.3 V s^{-1} and the voltage of the photomultiplier tube at 800 V.

RESULTS AND DISSCUSSION

Characterization of the Prepared MnS:CdS@ZnS QDs.

The morphology of the synthesized MnS:CdS@ZnS QDs was successfully analyzed. As seen in Figure 1A, MnS:CdS@ZnS QDs was uniformly dispersed with the size of 3 ± 0.2 nm by transmission electron microscopy (TEM) image. Furthermore, the analytical results showed that the approximate lattice spacing of MnS:CdS@ZnS QDs was 0.23 nm, which agrees well with previous literature[12] (Figure 1B). Meanwhile, the white line of the atomic force microscopy (AFM) image (Figure 1C) stated that the high profile was less than 1.5 nm, which indicated the monolayer of MnS:CdS@ZnS QDs (Figure 1D). In addition, the X-ray photoelectron spectroscopy (XPS) images of the MnS:CdS@ZnS QDs was analyzed to confirm the existence of several elements in Supporting Information (SI) Figure S1. As shown in SI Figure S1A, the results revealed five remarkable peaks at 161.14 eV, 284.44 eV, 404.3 eV, 532.08 eV, 652.08 eV, 1021.28 eV for S 2p, C 1s, Cd 3d, O 1s, Mn 2p, Zn 2p, respectively. Meanwhile, Mn 2p spectrum showed (SI Figure S1B) two evident peaks at 652.54 and 638.48 eV, which manifested that Mn 2p 1/2 and Mn 2p 3/2 existed.[12] After fitting the spectra of Cd 3d (SI Figure S1C), the pair of peaks in 404.27 eV was classified to Cd 3d 5/2 region, and the other peaks in 411 eV were assigned to the Cd 3d 3/2 region.[13] From SI Figure S1D, the XPS spectra of Zn 2p showed two peaks at 1021.27 and 1044.34 eV, which might be recognized as different Zn−O or Zn−S bonds in the crystalline lattice.[14] From SI Figure S1E, the XPS spectra of S

https://doi.org/10.1021/acs.analchem.2c00970
Anal. Chem. 2022, 94, 6874−6881

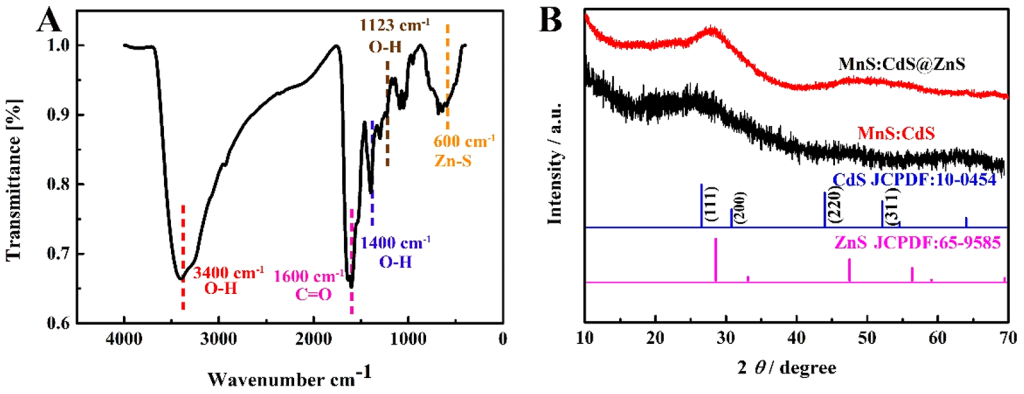

Figure 2. (A) The FTIR spectrum of MnS:CdS@ZnS QDs. (B) XRD patterns of MnS:CdS QDs (black line) and MnS:CdS@ZnS QDs (red line).

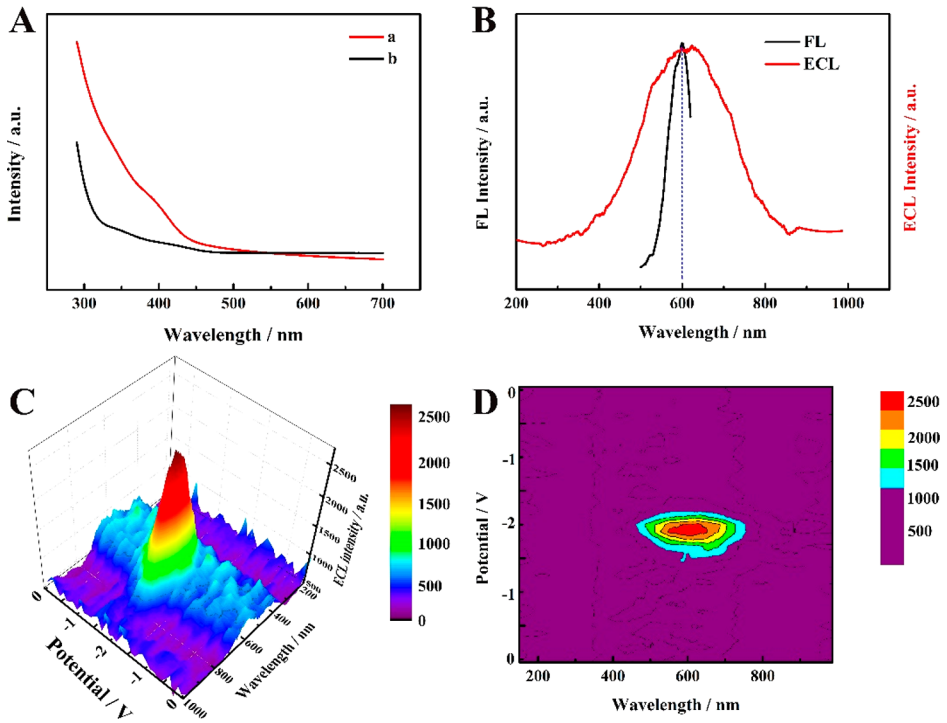

Figure 3. (A) UV absorption spectra of MnS:CdS@ZnS QDs (a) and CdS@ZnS QDs (b). (B) The FL spectra of MnS:CdS@ZnS QDs (black line) (Ex = 320 nm) and the ECL emission spectra of MnS:CdS@ZnS QDs in PBS solution containing 50 mM $K_2S_2O_8$ (red line). (C) The three-dimensional ECL spectra and (D) The ECL heat map of MnS:CdS@ZnS QDs.

2p showed peaks centered at 161 eV, 162 eV, and 163 eV, corresponding to interior S^{2-} and surface S atoms.[15] The XPS spectra of C 1s (SI Figure S1F) exhibited three peaks are at 285.14 eV, 286.49 eV, and 288.95 eV, which were, respectively, responsible for C−C, C−O, and C═O bonds.[16] Based on the above elemental analysis results, it was confirmed that MnS:CdS@ZnS QDs were successfully prepared.

The Fourier transform infrared spectra (FTIR) revealed the chemical bond of MnS:CdS@ZnS QDs (Figure 2A). The stretching vibration peaks at 3400 cm^{-1}, 1600 cm^{-1}, 1400 cm^{-1}, 1156 cm^{-1}, 1089 cm^{-1}, 954 cm^{-1}, and 681 cm^{-1} were assigned to O−H, C═O, O−H, C−O, O−H, Zn−S, respectively.[17] Additionally, the X-ray diffraction (XRD) images of MnS:CdS@ZnS QDs and MnS:CdS QDs were investigated to confirm the construction of core−shell structure. As exhibited in Figure 2B, the diffraction peaks showed the signature peaks of zinc blende CdS, which was coincident with JCPDF standard card 10-0454, indicating that the Mn-doping process did not change the crystal structure of the QDs. After adding the ZnS shell to MnS:CdS core, the diffraction peaks of MnS:CdS@ZnS QDs (red line) was toward the zinc blend structure ZnS (JCPDF:65-9585),[18] which demonstrated that the core−shell structure was successfully formed.

Based on Figure 3A, the UV absorption peak of CdS@ZnS QDs (curve b) was appeared in the wavelength range 320−450 nm. The absorption peak of MnS:CdS@ZnS QDs was at 400 nm (curve a), indicating that the Mn atoms were successfully doped in CdS@ZnS QDs to change the host lattice.[19] In addition, Figure 3B exhibited that the fluorescence emission peak of MnS:CdS@ZnS QDs was at 600 nm, and the obvious ECL emission peak of MnS:CdS@ZnS QDs was at 600 nm. It is worth noting that the ECL spectrum peak of MnS:CdS@ZnS QDs was identical to the PL spectrum peak with maximum emission at 600 nm, indicating that the surface state of MnS:CdS@ZnS QDs was highly passivated.[20] Besides, the

https://doi.org/10.1021/acs.analchem.2c00970
Anal. Chem. 2022, 94, 6874−6881

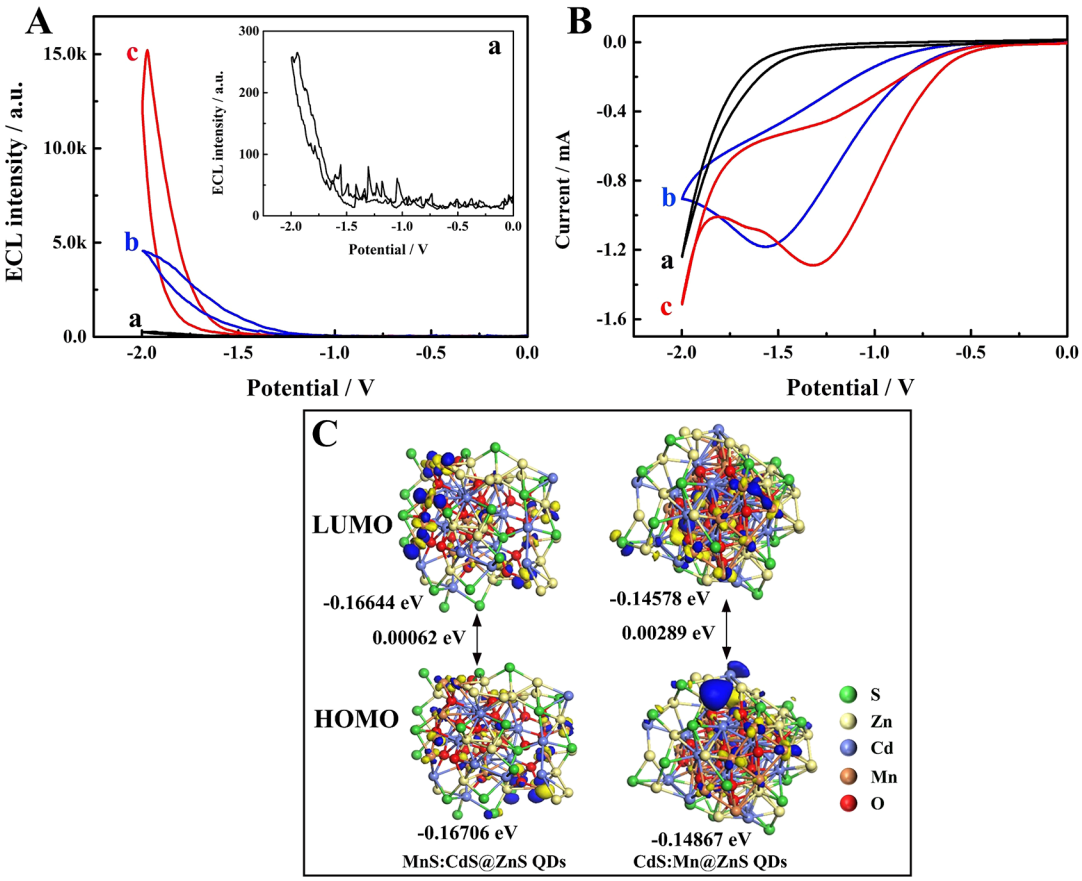

Figure 4. (A) ECL intensity−potential and (B) CV curves of MnS:CdS@ZnS QDs/GCE in PBS (curve a) and in 30 mM $S_2O_8^{2-}$ (curve c); CdS:Mn@ZnS QDs/GCE with 30 mM $S_2O_8^{2-}$ (curve b); (C) calculated molecular structure and energy levels for different QDs.

ECL three-dimension color map surface (Figure 3C) states that the ECL emission process continuously happened with the cyclic voltage scanning range of 0 V to −2 V and then back to 0 V with a maximum ECL emission potential at −2 V. Furthermore, in Figure 3D, the heat map image showed that the ECL emission wavelengths range of MnS:CdS@ZnS QDs was about 400−800 nm and emission peaks center was at 600 nm.

Comparation of ECL Response of the Two Types of QDs/$S_2O_8^{2-}$ system. As shown in Figure 4, to explore the possible different mechanism of two types of QDs (MnS:CdS@ZnS QDs through bimetallic clusters doping and CdS:Mn@ZnS QDs through ionic doping), ECL intensity and CV waves of two types of QDs modified GCE were investigated. The ECL response of MnS:CdS@ZnS QDs was less than 300 au(Figure 4A, a), owing to the absence of coreactant, which the corresponding CV response was weak apparently. Whereafter, in 30 mM $S_2O_8^{2-}$ solution, the phenomenon was observed that the ECL responses of MnS:CdS@ZnS QDs significantly zoomed to 15253.8 a.u (Figure 4A, c), which demonstrated that $S_2O_8^{2-}$ as coreactant could enhance the ECL response of MnS:CdS@ZnS QDs. Additionally, under the same experimental conditions, the ECL signal of CdS:Mn@ZnS QDs was also measured, which was only 4616.3 au (Figure 4A, b). Furthermore, in Figure 4B (curve b) displayed a reduction peak of CdS:Mn@ZnS QDs at −1.56 V, while the CV reduction wave of MnS:CdS@ZnS QDs showed a peak at −1.3 V (curve c), proving that the excitation energy of MnS:CdS@ZnS QDs was lower. As shown in Figure 4C, the calculation results of two types of QDs indicated that the energy gap value between the highest occupied molecular orbital (HOMO) and the lowest unoccupied molecular orbital (LUMO) of MnS:CdS@ZnS QDs was smaller than that of CdS:Mn@ZnS QDs. Admittedly, the smaller the energy gap is, the easier electrons on the HOMO jumps to LUMO for the generation of holes, which helps radical to rapidly inject holes to generate ECL emission.[21] More interestingly, the ECL efficiency of MnS:CdS@ZnS QDs (15.84%) was 18 times higher than that of CdS:Mn@ZnS QDs (0.87%) (the computational process displayed in the SI). Consequently, the higher ECL efficiency of MnS:CdS@ZnS QDs in the same experimental conditions was attributed to the neglect of dopants size mismatch and the elimination of "self-purification" effect. The ECL mechanism of MnS:CdS@ZnS QDs was elaborated in following. First, the MnS:CdS@ZnS QDs and $S_2O_8^{2-}$ obtained an electron and turned to MnS:CdS@ZnS QDs$^{\bullet-}$ and $SO_4^{\bullet-}$, respectively. Then the excited state (MnS:CdS@ZnS QDs*) was generated when MnS:CdS@ZnS QDs$^{\bullet-}$ reacted with $SO_4^{\bullet-}$, considerably improving ECL response of MnS:CdS@ZnS QDs.

$$\text{MnS: CdS@ZnS QDs} + e^- \rightarrow \text{MnS: CdS@ZnS QDs}^{\cdot-} \quad (1)$$

$$S_2O_8^{2-} + e^- \rightarrow SO_4^{2-} + SO_4^{\cdot-} \quad (2)$$

$$\text{MnS: CdS@ZnS QDs}^{\cdot-} + SO_4^{\cdot-} \rightarrow SO_4^{2-} + \text{MnS: CdS@ZnS QDs*} \quad (3)$$

$$\text{MnS: CdS@ZnS QDs*} \rightarrow \text{MnS: CdS@ZnS QDs} + h\nu \quad (4)$$

https://doi.org/10.1021/acs.analchem.2c00970
Anal. Chem. 2022, 94, 6874−6881

Polyacrylamide Gel Electrophoresis (PAGE) Analysis. The PAGE was adopted to confirm the successfulness of the designed target cycle amplification strategy. According to Figure 5, lanes 1−4 depicted four single chains, R, S, R*, and

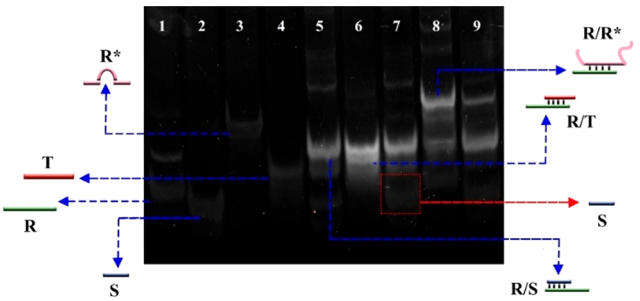

Figure 5. PAGE analysis of different samples. Lane 1, R; lane 2, S; lane 3, R*; lane 4, T; lane 5, R/S; lane 6, R/T; lane 7, R/S+T; lane 8, R/R*; lane 9, R/S+R*. The concentration of all samples is 1 μM.

T. Lanes 5, 6, and 8 showed the results for the hybridization of R/S, R/T, R/R*, respectively. In lane 7, the results of the reaction about T with R/S were identical with lanes 6 and 2, which demonstrated that T displaced S to form R/T for the release of S (red dotted box). In lane 9, by adding R* to R/S, the lane corresponded to lanes 3 and 8, which indicated that R* did not react with the duplex of R*/S. To verify the release of R*, the PAGE results are shown in SI Figure S2A. Three single strands in lanes 1−3 were referred to as R*, F*, and F, respectively. When R* and F* were hybridized by annealing (R*/F*), lane 4 exhibited a bright band. Lane 5 showed two distinct bands of R* and F/F*, which was in accordance with lanes 1 and 6, suggesting that F could hybridize with F* to release R*. As shown in SI Figure S2B, three single strands in lanes 1−3 were referred to as R, T, and R*, respectively. Lanes 4 and 5 showed R/T duplex and R/R* duplex. After adding R* into the R/T duplex, two bands of R/R* and T were observed (lane 6), which showed that R* recognized R/T duplex and released T to participate in the cycle. Therefore, the above results confirmed that the F-powered target cycling amplification occurred as expected.

Detection of the Designed Biosensor for MiRNA Let-7a. The quantitative measurement of the constructed biosensor for miRNA let-7a with various concentration was performed under the optimized conditions (SI Figure S5) by "signal on−off" mode. The ECL intensity gradually increased from 1 nM to 10 aM as changed miRNA let-7a concentration (Figure 6A). Based on the good linear relationship of ΔI_{ECL} (the changes values between blank values and obtained values) with the logarithm of target concentration, the linear regression equation was calculated as ΔI = 16947.65 + 942.64 lg$c$ (R^2 = 0.998, R referred to correlation coefficient) with the detection limit of 4.1 aM (the relevant calculation process shown in the n SI). Impressively, this proposed "signal on−off" ECL biosensor exhibited wider detection range and higher sensitivity than the previous reports. (Table 1)

Table 1. Designed Biosensor Compared with Other Works for MiRNA let-7a Detection

measurement technique	linear range	LOD	Reference
fluorescence	100 aM ~ 10 nM	84.5 aM	22
electrochemical	10 fM ~ 50 nM	5.1 fM	23
SERS	10 aM ~ 10 nM	5.3 aM	24
colorimetric	50 pM ~ 10 nM	21.7 pM	25
ECL	10 fM ~ 100 nM	4.92 fM	26
ECL	10 fM ~ 10 nM	1.49 fM	27
ECL	10 aM ~ 1 nM	4.1 aM	this work

Selectivity and Stability of the Designed ECL Biosensor for MiRNA let-7a. The selectivity was regarded as one of the important criterions in assessing constructed sensors performance, so other RNAs were choose as interferents. As shown in Figure 7A, three interfering substances (miRNA-21, thymidine kinase 1 (TK1) mRNA and miRNA-141) were adopted to substitute miRNA let-7a. As we can see, the ECL intensity of miRNA-21 (10 pM), TK1 mRNA (10 pM) and miRNA-141 (10 pM) was inappreciably different from that of the blank sample, suggesting that the developed biosensor possessed excellent selectivity and specificity. Furthermore, in Figure 7B, the stable ECL responses could be observed by consecutive 10 cycles ECL scans with RSD of 1.98% (1 fM) and 3.25% (10 pM), respectively. According to the performs of proposed biosensor, we concluded that the biosensing possessed excellent stability and outstanding selectivity, which could be further applied in bioassay.

Applied Performs of the Biosensor in Cancer Cells. In order to prove the practical application ability of the designed sensor for miRNA let-7a in real samples, the cell lysates of

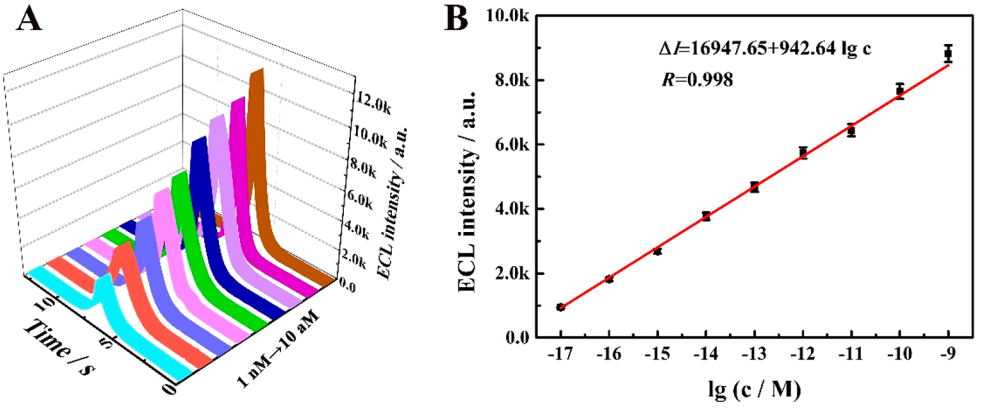

Figure 6. (A) ECL biosensors intensity of various miRNA let-7a concentrations range of 10 aM to 1 nM. (n = 3) (B) Calibration curve for different miRNA let-7a concentrations.

https://doi.org/10.1021/acs.analchem.2c00970
Anal. Chem. 2022, 94, 6874−6881

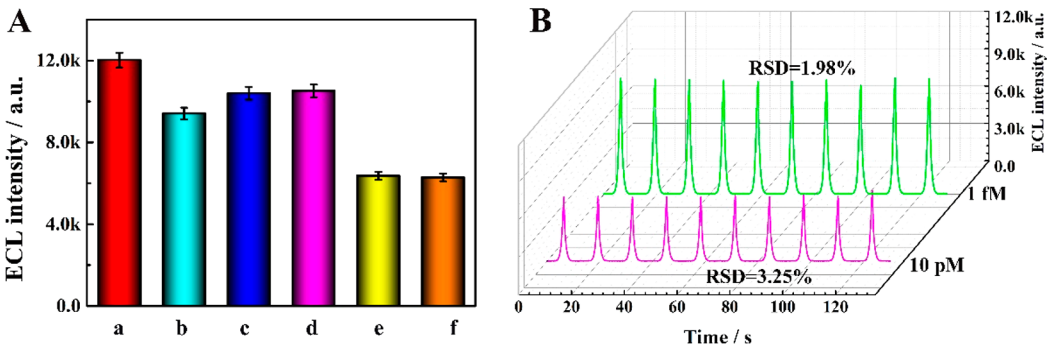

Figure 7. (A) The selectivity study of the biosensing with interferents (a) blank, (b) miRNA-21 (10 pM), (c) TK1 mRNA (10 pM), (d) miRNA-141 (10 pM), (e) mixture solution (containing miRNA let-7a, miRNA-21, TK1 mRNA, miRNA-141), (f) miRNA let-7a (1 pM). Error bars, SD, n = 3. (B) The stability study of the biosensor detected with 1 fM and 10 pM miRNA let-7a by continuous scanning 10 cycles.

MCF-7 and A549 were employed to evaluate the expression of miRNA let-7a in tumor cells. In Figure 8, the ECL behavior

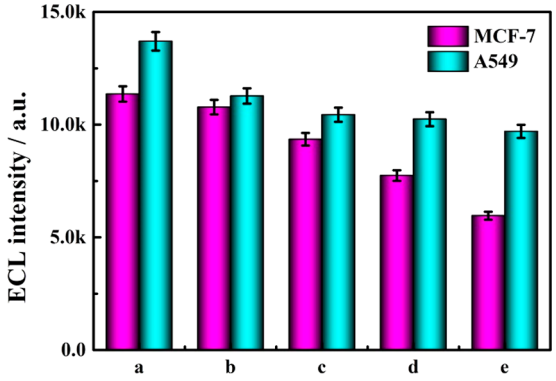

Figure 8. Corresponding ECL responses of the biosensor in A549 and MCF-7 cells lysates at cells concentrations from 10^1 (a) to 10^5(e).

was changed drastically when the cells concentration of MCF-7 was changed from 10^1 cells to 10^5 cells, which meant that miRNA let-7a was the high expression in MCF-7. However, the ECL responses of the proposed biosensor exhibited slight decrease at different number cells of A549, which illustrate that miRNA let-7a was the low expression in A549. The results were consistent with previously reported literature[27] and implied that the developed biosensor had the potential in detection miRNA let-7a from cancer cells.

CONCLUSIONS

In this work, we designed a novel ECL biosensing platform using MnS:CdS@ZnS QDs and mRNA powered strand amplification reaction for miRNA let-7a detection. Interestingly, MnS:CdS@ZnS QDs with bimetallic clusters doping were successfully synthesized as ECL emitters to make the obliteration of the dopants size mismatch and avoid the defects of "self-purification" effect for an intense ECL emission with the ECL efficiency of 15.84% with $S_2O_8^{2-}$ as the coreactant. Significantly, mRNA-powered strand displacement amplification as signal amplification strategy was initiated to export a large amount of output DNA modified with ferrocene (Fc), which were captured simultaneously on the electrode to form "Y" structure with the aid of Probe DNA1 and Probe DNA2, giving rise to declined ECL intensity as "signal-off" state. Significantly, the improved ECL "signal on−off" mode biosensor is in possession of the limit of detection as low as 4.1 aM, which offers a preeminent strategy for sensitive detection of biomolecules in cancer cells.

ASSOCIATED CONTENT

Supporting Information

The Supporting Information is available free of charge at https://pubs.acs.org/doi/10.1021/acs.analchem.2c00970.

Sequence information of the nucleic acids, preparation of Ag nanoparticles, preparation of ionic doping QDs, ECL efficiency calculation procedure of different QDs, the experimental procedure of PAGE, XPS spectra, the results of PAGE, ECL behaviors comparison of different types of Mn doped CdS QDs, CV characterization, optimal conditions for the ECL biosensor, zeta potential, and the calculation of limit of detection (PDF)

AUTHOR INFORMATION

Corresponding Authors

Ruo Yuan − *Key Laboratory of Luminescence Analysis and Molecular Sensing (Southwest University), Ministry of Education, College of Chemistry and Chemical Engineering, Southwest University, Chongqing 400715, PR China;* orcid.org/0000-0003-3664-6236; Phone: +86-23-68252277; Email: yuanruo@swu.edu.cn; Fax: +86-23-68253172

Ya-Qin Chai − *Key Laboratory of Luminescence Analysis and Molecular Sensing (Southwest University), Ministry of Education, College of Chemistry and Chemical Engineering, Southwest University, Chongqing 400715, PR China;* orcid.org/0000-0003-4392-9592; Phone: +86-2368252277; Email: yqchai@swu.edu.cn; Fax: +86-2368253172

Authors

Yu-Ting Yang − *Key Laboratory of Luminescence Analysis and Molecular Sensing (Southwest University), Ministry of Education, College of Chemistry and Chemical Engineering, Southwest University, Chongqing 400715, PR China*

Jia-Li Liu − *Key Laboratory of Luminescence Analysis and Molecular Sensing (Southwest University), Ministry of Education, College of Chemistry and Chemical Engineering, Southwest University, Chongqing 400715, PR China*

Man-Fei Sun − *Key Laboratory of Luminescence Analysis and Molecular Sensing (Southwest University), Ministry of Education, College of Chemistry and Chemical Engineering, Southwest University, Chongqing 400715, PR China*

https://doi.org/10.1021/acs.analchem.2c00970
Anal. Chem. 2022, 94, 6874−6881

Complete contact information is available at:
https://pubs.acs.org/10.1021/acs.analchem.2c00970

Notes

The authors declare no competing financial interest.

■ ACKNOWLEDGMENTS

This work was financially supported by the National Natural Science Foundation (NNSF) of China (21974108, 22176153, and 22174113) and Chongqing Postdoctoral Innovative Talent Support Program (7820100788).

■ REFERENCES

(1) Xian, L.; Xu, F.; Liu, J.; Xu, N.; Li, H.; Ge, H.; Shao, K.; Fan, J.; Xiao, G.; Peng, X. *J. Am. Chem. Soc.* **2019**, *141*, 20490−20497.
(2) Zanut, A.; Fiorani, A.; Canola, S.; Saito, T.; Ziebart, N.; Rapino, S.; Rebeccani, S.; Barbon, A.; Irie, T.; Josel, H. P.; Negri, F.; Marcaccio, M.; Windfuhr, M.; Imai, K.; Valenti, G.; Paolucci, F. *Nat. Commun.* **2020**, *11*, 2668.
(3) Liu, X. H.; Li, L. B.; Luo, L. J.; Bi, X. Y.; Zhao, W. L.; Yan, H.; Li, X.; You, T. Y. *Biosens. Bioelectron.* **2021**, *184*, 113232.
(4) Jiang, D.; Wei, M.; Du, X. J.; Qin, M.; Shan, X. L.; Chen, Z. D. *Chem. Eng. J.* **2022**, *430*, 132771.
(5) Xiao, S. Y.; Wang, X. Y.; Yang, C. P.; Jiang, Y. J.; Zhen, S. J.; Huang, C. Z.; Li, Y. F. *Anal. Chem.* **2022**, *94*, 1178−1186.
(6) Li, Y.; Liu, D.; Meng, S.; Zhang, J.; Li, L.; You, T. *Anal. Chem.* **2022**, *94*, 1294−1301.
(7) Xiong, H. W.; Huang, Z. P.; Lin, Q. Y.; Yang, B.; Yan, F.; Liu, B. H.; Chen, H.; Kong, J. L. *Anal. Chem.* **2022**, *94*, 837−846.
(8) Norris, D. J.; Efros, A. L.; Erwin, S. C. *Science.* **2008**, *319*, 1776−1779.
(9) Lu, H. P.; Carroll, G. M.; Chen, X. H.; Amarasinghe, D. K.; Neale, N. R.; Miller, E. M.; Sercel, P. C.; Rabuffetti, F. A.; Efros, A. L.; Beard, M. C. *J. Am. Chem. Soc.* **2018**, *140*, 13753−13763.
(10) Zhang, H.; Yu, J. L.; Sun, C. X.; Xu, W. H.; Chen, J.; Sun, H.; Zong, C.; Liu, Z.; Tang, Y.; Zhao, D. Y. *J. Am. Chem. Soc.* **2020**, *142*, 16177−16181.
(11) Liu, J. L.; Yang, R.; Chai, Y. Q.; Yuan, R. *Anal. Chem.* **2021**, *93*, 13334−13341.
(12) Cao, Z. Y.; Shu, Y. F.; Qin, H. Y.; Su, B.; Peng, X. G. *ACS Cent Sci.* **2020**, *6*, 1129−1137.
(13) Du, D. X.; Shu, J. N.; Guo, M. Q.; Haghighatbin, M. A.; Yang, D.; Bian, Z. P.; Cui, H. *Anal. Chem.* **2020**, *92*, 14113−14121.
(14) Elnaz, J. M.; Zahra, S. *Appl. Surf. Sci.* **2018**, *441*, 1−11.
(15) Hewa-Rahinduwage, C. C.; Geng, X.; Silva, K. L.; Niu, X. F.; Zhang, L.; Brock, S. L.; Luo, L. *J. Am. Chem. Soc.* **2020**, *142*, 12207−12215.
(16) Sun, M. F.; Liu, J. L.; Zhou, Y.; Zhang, J. Q.; Chai, Y. Q.; Li, Z. H.; Yuan, R. *Anal. Chem.* **2020**, *92*, 14723−14729.
(17) Jonnalagadda, M.; Prasad, V. B.; Raghu, A. V. *J. Mol. Struct.* **2021**, *1230*, 129875.
(18) Li, Z. J.; Hofman, E.; Blaker, A.; Davis, A. H.; Dzikovski, B.; Ma, D. K.; Zheng, W. *ACS Nano* **2017**, *11*, 12591−12600.
(19) Hofman, E.; Robinson, R. J.; Li, Z. J.; Dzikovski, B.; Zheng, W. *J. Am. Chem. Soc.* **2017**, *139*, 8878−8885.
(20) He, Y. P.; Hou, S. F.; Yang, L. Q.; Zhang, F.; Zou, G. Z. *Chemistry* **2018**, *24*, 9592−9597.
(21) Zhang, X.; Zhang, B.; Miao, W. J.; Zou, G. Z. *Anal. Chem.* **2016**, *88*, 5482−5488.
(22) Li, C. C.; Hu, J. P.; Zou, X. R.; Luo, X. L.; Zhang, C. Y. *Anal. Chem.* **2022**, *94*, 1882−1889.
(23) Wang, D.; Chai, Y. Q.; Yuan, Y. L.; Yuan, R. *Anal. Chem.* **2020**, *92*, 14197−14202.
(24) Kang, T. L.; Zhu, J. T.; Luo, X. J.; Jia, W. Y.; Wu, P.; Cai, C. X. *Anal. Chem.* **2021**, *93*, 2519−2526.
(25) Chen, W. W.; Zhang, X. B.; Li, J. J.; Chen, L. Z.; Wang, N. N.; Yu, S. Q.; Li, G. M.; Xiong, L. F.; Ju, H. X. *Anal. Chem.* **2020**, *92*, 2714−2721.
(26) Liao, N.; Pan, M. C.; Wang, L.; Yang, F.; Yuan, R.; Zhuo, Y. *Anal. Chem.* **2021**, *93*, 4051−4058.
(27) Zhao, M. L.; Zeng, W. J.; Chai, Y. Q.; Yuan, R.; Zhuo, Y. *Anal. Chem.* **2020**, *92*, 11044−11052.

Recommended by ACS

Ultrasensitive Photoelectrochemical Biosensor Based on Novel Z-Scheme Heterojunctions of Zn-Defective CdS/ZnS for MicroRNA Assay
Xiankang Niu, Weihong Tan, *et al.*
DECEMBER 16, 2021
ANALYTICAL CHEMISTRY
READ

Novel Ultrasensitive Photoelectrochemical Cytosensor Based on Hollow $CdIn_2S_4/In_2S_3$ Heterostructured Microspheres for HepG2 Cells Detection and Inhibitor Screening
Jing-Jing Wei, Jiu-Ju Feng, *et al.*
AUGUST 22, 2022
ANALYTICAL CHEMISTRY
READ

Novel Ratiometric Electrochemiluminescence Biosensor Based on BP-CdTe QDs with Dual Emission for Detecting MicroRNA-126
Jinwen Zhao, Ruo Yuan, *et al.*
SEPTEMBER 01, 2021
ANALYTICAL CHEMISTRY
READ

Silica-Coated Silver Nanoparticles Decorated with Fluorescent CdTe Quantum Dots and DNA Aptamers for Detection of Tetracycline
Xueqing Wang, He Huang, *et al.*
AUGUST 30, 2020
ACS APPLIED NANO MATERIALS
READ

Get More Suggestions >